

# Analysis of liquid-to-solid coupling and other performance parameters for microfluidically reconfigurable photonic systems

Erica E. Jung, Aram J. Chung,  
and David Erickson\*

*Sibley School of Mechanical and Aerospace Engineering, Cornell University, Ithaca, NY 14853 USA*  
*\*de54@cornell.edu*

**Abstract:** In this paper, we analytically investigate the coupling of light from liquid-core waveguides to conventional solid-core waveguides and a series of other optical properties of liquid waveguides in order to gauge the practicality of such a system for use in microfluidically reconfigurable photonic systems. A finite element model of the system was constructed and relevant properties such as mode field diameter, attenuation, bending loss, and efficiency of evanescent and end-fire coupling were investigated as a function of the liquid waveguide Peclet number and the relative difference in refractive index. For pure liquid systems we show that the mode field diameter decreases monotonically with increasing Peclet number and that bending losses could be significantly reduced by increasing the Peclet number. More critically, we observed irreversible evanescent coupling, in which the light coupled in the solid waveguide is entrapped within the solid rather than coupled back into the liquid waveguide. This effect was caused by the lengthwise variation in the propagation constant of the liquid core due to downstream diffusion. We demonstrate that coupling efficiencies as high as 84% can be obtained for fluid based end-fire coupling by taking advantage of the tunable mode field diameter. By developing techniques for coupling light between liquid and solid states we hope to be able to overcome the drawbacks of solid waveguide systems (*e.g.* unchangeable structure and properties) and liquid waveguide systems (*e.g.* diversion and attenuation) yielding a new paradigm for reconfigurable photonics.

©2010 Optical Society of America

**OCIS codes:** (230.7370) Waveguides; (130.2790) Guided waves; (130.3120) Integrated optics devices; (060.1810) Couplers;

---

## References and Links

1. D. Psaltis, S. R. Quake, and C. H. Yang, "Developing optofluidic technology through the fusion of microfluidics and optics," *Nature* **442**(7101), 381–386 (2006).
2. C. Monat, P. Domachuk, and B. J. Eggleton, "Integrated optofluidics: A new river of light," *Nat. Photonics* **1**(2), 106–114 (2007).
3. A. Ymeti, J. Greve, P. V. Lambeck, T. Wink, S. W. van Hövell, T. A. M. Beumer, R. R. Wijn, R. G. Heideman, V. Subramaniam, and J. S. Kanger, "Fast, ultrasensitive virus detection using a Young interferometer sensor," *Nano Lett.* **7**(2), 394–397 (2007).
4. X. L. Mao, S. C. S. Lin, M. I. Lapsley, J. J. Shi, B. K. Juluri, and T. J. Huang, "Tunable Liquid Gradient Refractive Index (L-GRIN) lens with two degrees of freedom," *Lab Chip* **9**(14), 2050–2058 (2009).
5. X. Q. Cui, L. M. Lee, X. Heng, W. W. Zhong, P. W. Sternberg, D. Psaltis, and C. H. Yang, "Lensless high-resolution on-chip optofluidic microscopes for *Caenorhabditis elegans* and cell imaging," *Proc. Natl. Acad. Sci. U.S.A.* **105**(31), 10670–10675 (2008).
6. S. Mandal, X. Serey, and D. Erickson, "Nanomanipulation using silicon photonic crystal resonators," *Nano Lett.* **10**(1), 99–104 (2010).

7. A. H. J. Yang, S. D. Moore, B. S. Schmidt, M. Klug, M. Lipson, and D. Erickson, "Optical manipulation of nanoparticles and biomolecules in sub-wavelength slot waveguides," *Nature* **457**(7225), 71–75 (2009).
8. D. B. Wolfe, R. S. Conroy, P. Garstecki, B. T. Mayers, M. A. Fischbach, K. E. Paul, M. Prentiss, and G. M. Whitesides, "Dynamic control of liquid-core/liquid-cladding optical waveguides," *Proc. Natl. Acad. Sci. U.S.A.* **101**(34), 12434–12438 (2004).
9. Z. Y. Li, Z. Y. Zhang, A. Scherer, and D. Psaltis, "Mechanically tunable optofluidic distributed feedback dye laser," *Opt. Express* **14**(22), 10494–10499 (2006).
10. X. C. Li, J. Wu, A. Q. Liu, Z. G. Li, Y. C. Soew, H. J. Huang, K. Xu, and J. T. Lin, "A liquid waveguide based evanescent wave sensor integrated onto a microfluidic chip," *Appl. Phys. Lett.* **93**(19), 193901–193903 (2008).
11. J. M. Lim, S. H. Kim, J. H. Choi, and S. M. Yang, "Fluorescent liquid-core/air-cladding waveguides towards integrated optofluidic light sources," *Lab Chip* **8**(9), 1580–1585 (2008).
12. M. Rosenauer, and M. J. Vellekoop, "A versatile liquid-core/liquid-twin-cladding waveguide micro flow cell fabricated by rapid prototyping," *Appl. Phys. Lett.* **95**(16), 163702–163705 (2009).
13. H. G. Park, C. J. Barrelet, Y. N. Wu, B. Z. Tian, F. Qian, and C. M. Lieber, "A wavelength-selective photonic-crystal waveguide coupled to a nanowire light source," *Nat. Photonics* **2**(10), 622–626 (2008).
14. J. S. Levy, A. Gondarenko, M. A. Foster, A. C. Turner-Foster, A. L. Gaeta, and M. Lipson, "CMOS-compatible multiple-wavelength oscillator for on-chip optical interconnects," *Nat. Photonics* **4**(1), 37–40 (2010).
15. A. J. Chung, E. Jung, and D. Erickson, "A new form of reconfigurable material using optofluidic waveguides", in *Proceedings of Micro- Total Analysis System*, (Jeju, Korea, 2009), pp. 198–200.
16. D. Lide, ed., *Handbook of Chemistry of Physics*, 79th ed. (CRC Press, 1999).
17. D. Marcuse, "TE modes of graded-index slab waveguides," *IEEE J. Quantum Electron.* **9**(10), 1000–1006 (1973).
18. C. R. Pollock, *Fundamentals of Optoelectronics* (Richard D. Irwin, INC., 1995).
19. S. Kawakami, M. Miyagi, and S. Nishida, "Bending losses of dielectric slab optical waveguide with double or multiple claddings: theory," *Appl. Opt.* **14**(11), 2588–2597 (1975).
20. K. Thyagarajan, M. R. Shenoy, and A. K. Ghatak, "Accurate numerical method for the calculation of bending loss in optical waveguides using a matrix approach," *Opt. Lett.* **12**(4), 296–298 (1987).
21. C. H. Tsai, C. H. Tai, L. M. Fu, and F. B. Wu, "Experimental and numerical analysis of the geometry effects of low-dispersion turns in microfluidic systems," *J. Micromech. Microeng.* **15**(2), 377–385 (2005).
22. A. W. Snyder, and J. D. Love, *Optical waveguide Theory* (Chapman and Hall, 1983).
23. K. S. Chiang, and S. Y. Cheng, "Technique of applying the prism-coupler method for accurate measurement of the effective indices of channel waveguides," *Opt. Eng.* **47**(3), 034601–034604 (2008).
24. B. Wang, J. H. Jiang, and G. P. Nordin, "Compact slanted grating couplers," *Opt. Express* **12**(15), 3313–3326 (2004).
25. V. R. Almeida, R. R. Panepucci, and M. Lipson, "Nanotaper for compact mode conversion," *Opt. Lett.* **28**(15), 1302–1304 (2003).

---

## 1. Introduction

Since its inception, Optofluidics [1,2], or the fusion of microfluidics with optics, has had significant impact in a number of areas including: optical biosensors, lensing and imaging [3–5], nanomanipulation [6,7] and on-chip waveguiding and lasing [8,9]. A popular approach to the latter of these is through the use of liquid core/fluid cladding waveguides [10–12] which represent a new type of optical element whereby a high refractive index liquid is cladded by a lower refractive index fluid are used to guide light around on a microfluidic chip. Compared to conventional solid waveguides, liquid waveguides have a number of significant advantages including: physical adaptability (*i.e.* the light path or mode profile can be reconfigured on command simply by adjusting the local flow conditions), chemical adaptability (*i.e.* varying levels of gain media or non-linear solutions can be introduced to or removed from the waveguide) and thermal stabilization. Despite these advantages, liquid state optical components are not likely to ever completely replace solid state optical components due to limitations in switching speed, general robustness and lack of advanced functionality such as active filtering or electro-optic modulation [13,14].

Recently we have proposed a new approach to reconfigurable photonics which allows us to take advantage of the chemical and physical adaptability of liquid state photonics with the robustness and speed available from traditional solid state photonics [15]. By combining liquid and planar solid state components on a chip, it is possible to establish a new optical platform which is not only flexible and reconfigurable, but also fast, stable and easy to operate. As we discuss in further detail below, since both the solid and liquid state elements are reasonably well developed, the major challenge in realizing this platform is in the

development of technique that allows one to transfer light from the liquid state to the solid state and back again. While numerous experimental studies of liquid waveguides have been performed [8–12], to date little theoretical work has been done to characterize the performance parameters of these devices, particularly related to liquid-solid coupling.

In this paper, we present a comprehensive analytical and numerical study of the use of liquid state elements in reconfigurable photonics. In the first part of the paper we use a coupled hydrodynamic-electromagnetic finite element model (FEM) to analyze liquid state behavior as a function of waveguide Peclet number, including mode field diameter and bending loss. The second part of the paper focuses on investigating both evanescent and end-fire liquid-to-solid optical coupling schemes. In addition to characterizing the coupling efficiency and length as a function of waveguide Peclet number, uniquely fluid-optical effects are demonstrated including irreversible evanescent coupling and dynamic mode field matching.

## 2. Theory

To obtain the refractive index (RI) profile in the liquid waveguide, we first have to determine the flow velocity field and concentration profile of the solution dopant used to create the waveguide core. Once the RI profile is known the wave equation can be used to model the light propagation along the waveguide. In this section we provide details of the numerical method used to simulate the system.

### 2.1. Diffusion of liquid core in liquid waveguide

Instead of the step change in RI between the core and cladding as in a solid core waveguide, a liquid waveguide has a continuous distribution of RI which is caused by diffusion of the liquid core dopant into the cladding. The direction of the diffusion occurs both perpendicular to the direction of optical propagation, as with a conventional graded index waveguides, as well as parallel with it. To obtain the RI profile the fluid dynamical continuity and conservation of momentum equations in steady state, Eq. (1a) and (1b), must first be solved to obtain the velocity field. Once the velocity field is obtained it can be used as an input into the steady state convection-diffusion equation, Eq. (2), to obtain the concentration profile  $c$ . Once the concentration profile is obtained, the RI profile can be obtained directly from experimentally obtained values (solutions of calcium chloride,  $\text{CaCl}_2$ , were used in this study which ranges in refractive index from deionized water ( $n = 1.33$ ) to 5M ( $n = 1.44$ ) [16]).

$$\nabla \cdot \mathbf{v} = 0 \quad (1a)$$

$$\rho \mathbf{v} \cdot \nabla \mathbf{v} = -\nabla p + \mu \cdot \nabla^2 \mathbf{v} \quad (1b)$$

$$\mathbf{v} \cdot \nabla c = D \nabla^2 c \quad (2)$$

In Eq. (1a) and (1b)  $\mathbf{v}$ ,  $\rho$ ,  $p$ , and  $\mu$  are velocity vector, fluid density, pressure and viscosity respectively. In Eq. (2),  $c$  and  $D$  are the concentration and the mass diffusion coefficient. We can nondimensionalize Eq. (1b) and (2) by considering reference parameters  $V$  and  $L$ , average velocity and length scale. In Eq. (3a) and (4a), nondimensional variables are denoted by starred properties:  $\mathbf{v}^* = \mathbf{v} / V$ ,  $p^* = \mu V / L$ ,  $\nabla^* = \nabla \cdot L$ ,  $\nabla^{*2} = \nabla \cdot L^2$ .

$$Re \cdot (\mathbf{v}^* \cdot \nabla^* \mathbf{v}^*) = -\nabla^* p^* + \nabla^{*2} \mathbf{v}^* \quad (3a)$$

$$Re = \rho V L / \mu \quad (3b)$$

$$Pe \cdot (\mathbf{v}^* \cdot \nabla^* c) = \nabla^{*2} c \quad (4a)$$

$$Pe = V L / D \quad (4b)$$

Where  $Re$  and  $Pe$  are the Reynolds number and Peclet number respectively. The Reynolds number, Eq. (3b), is a ratio of inertial forces to viscous forces. In micro scale flows, the left hand side of the Eq. (3a) can be ignored and two dominant parameters, the pressure and viscosity, cause laminar flow ( $Re$  used in this paper was in the range of 0.1 ~1). The Peclet number, Eq. (4b), is a ratio of convective transport to diffusive transport. The increase of Peclet number means that diffusive mixing of fluids in the channel is reduced. Thus liquid waveguides with higher Peclet numbers would be expected to experience less downstream broadening.

## 2.2. Light propagation in liquid waveguide

Once the refractive index profile is obtained, the wave equation can be solved to obtain solutions of light propagation within the waveguide. Under the assumption of the negligibly small gradient in the permittivity of the medium, the wave equation can be expressed as

$$\nabla_t^2 E_t + (k_0^2 n_t^2 - \beta^2) E_t = 0 \quad (5)$$

where  $\nabla_t$ ,  $E_t$ ,  $k_0$ ,  $n_t$  and  $\beta$  are the transverse part of  $\nabla$ , the transverse electric field, the free-space wavenumber, the refractive index of the medium and the propagation constant respectively. Previous studies of conventional graded index waveguides [17] had rigid solid boundaries and diffusion layers only in the direction perpendicular to propagation. As alluded to above, in the case of liquid waveguide however the refractive index profile also changes along the direction of optical propagation. In the case where the flow is unconfined into a free solution it may be possible to obtain an analytical solution to the above set of equations. For the more generally applicable case where the waveguide is confined within a microchannel or near a surface such a solution is not possible and numerical techniques must be used.

## 2.3. Numerical method and boundary conditions

We performed detailed numerical simulations of light propagation in liquid waveguides and optical coupling from the liquid to the solid waveguide using a commercial finite element code. Figure 1 is a schematic of the elements of the liquid waveguide system we modeled here. Fluid flow was introduced by the pressure gradient between inlets, (1) and (2) in Fig. 1, and the outlet. Incompressible flow, constant viscosity and no slip boundary conditions at solid walls were assumed to compute the flow field. As mentioned above, we used solution of  $\text{CaCl}_2$  (5M,  $n = 1.44$ ) as the core solution. In all cases the core was focused into the microchannel between two cladding streams of DI water ( $n = 1.33$ ) under the assumption of no reaction in the channel. Once we obtain the concentration profile, the transverse electric (TE) mode polarized along the Z-direction was excited at the inlet of the core stream. The output boundary of the liquid waveguide was terminated by a perfectly matched layer. The simulations of the flow, concentration and electromagnetic fields were decoupled; thus each of the simulations was solved independently in the sequence of the flow field, concentration field and electromagnetic field.

As has been previously demonstrated [8], the cladding liquids with low RI sandwich the core liquid with high RI to obtain total internal refraction of the light within the liquid waveguide. Liquid waveguides were designed to be 1.5  $\mu\text{m}$  wide at the inlet in order to support only the fundamental TE mode at a working wavelength of 1550 nm. Total length of the microchannel used in the paper is 500 $\mu\text{m}$  and the width is 20 $\mu\text{m}$ . Peclet numbers analyzed in this paper are in the range from 100 to 1000 and flow rates corresponding to the Peclet numbers are in the range from 0.005m/s to 0.05m/s. All simulations done in this paper are done using a 2D computational domain, which we believe is sufficient to capture the essential physics of the waveguide characterization and coupling parameters of interest here. Out of plane influences such as: the additional diffusive transport of the waveguide core, the 3D shape the liquid waveguide would assume as it interacted with a ridge waveguide, and the

more complex velocity patterns which result from the presence of an upper and lower surfaces (in particular the generation of Dean's vortices for curved channels at high flow velocities) would not be fully captured by our model. The latter of these limitations is discussed in more detail in section 3.2.

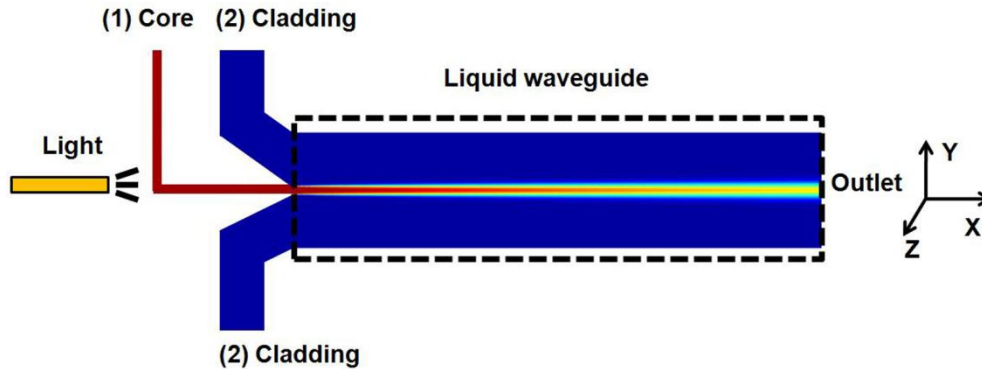


Fig. 1. Schematic diagram of the liquid waveguide. Dotted area was simulated in this paper

### 3. Results and discussion: light propagation in liquid waveguide

As described in detail in section 2.1, the diffusive behavior of the waveguide (and consequently its local refractive index profile) is governed by the magnitude of the transport Peclet number. By extension then, it is reasonable to expect that both the optical performance and waveguide characteristics will both be strongly dependent on the Peclet number. As a result, prior to beginning our detailed analysis of the coupling between liquid and solid core systems, we will examine in detail how relevant optical properties such as mode field diameter (MFD), attenuation, and bending loss are dependent on it.

#### 3.1. Mode field diameter and attenuation

For the case of interest here the Mode Field Diameter (MFD) [18] is representative of how tightly light is confined within the waveguide. Generally speaking the lower the index contrast between the core and the cladding of the waveguide, the larger the MFD. In the case of the liquid waveguide, the contrast of the refractive indices of the core liquid and cladding liquid becomes lower as the core liquid diffuses as it is transported downstream resulting in an ever increasing MFD along the length of the waveguide. The effect is illustrated in Fig. 2(a) and 2(b), which shows the refractive index and the steady state electric field profiles at  $Pe = 200$ , and Fig. 2(c) and 2(d), which shows the refractive index and the steady state electric field profiles at  $Pe = 800$ . Figure 2(e) and 2(f) show the power intensity distribution at the distance  $300\mu\text{m}$  apart from the inlet,  $Pe = 200$  and  $800$  respectively.

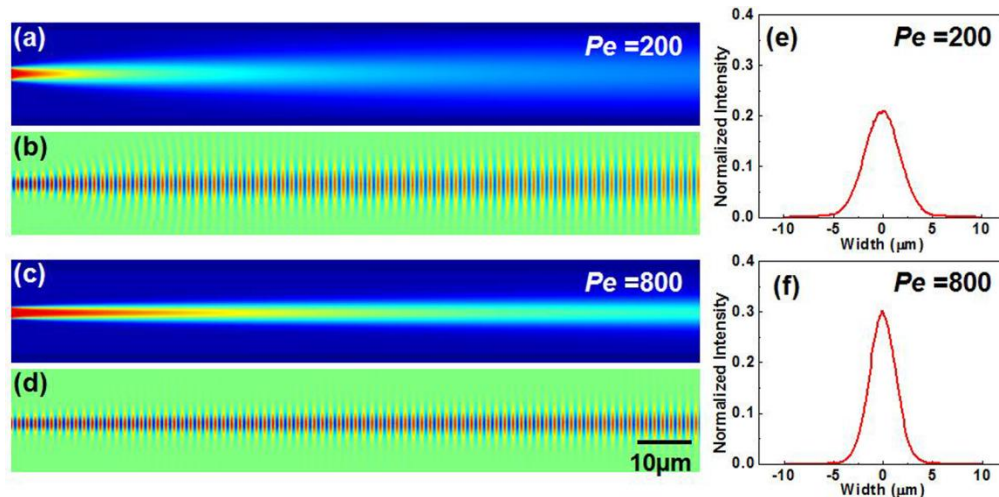


Fig. 2. (a, b) Refractive index and steady state electric field profiles at  $Pe = 200$ . (c, d) Refractive index and steady state electric field profiles at  $Pe = 800$ . (e, f) Power intensity distribution at a downstream distance of  $300\mu\text{m}$ ,  $Pe = 200$  and  $800$  respectively.

Figure 3(a) plots the MFD along the liquid waveguide at different Peclet numbers. MFD was estimated at the point that intensity dropped to  $1/e^2$  of its maximum. As shown below, higher Peclet number resulted in a less dilute liquid core, and therefore a smaller mode field diameter (*e.g.* MFD at  $Pe = 800$  was  $6\mu\text{m}$  while MFD at  $Pe = 200$  was  $8.4\mu\text{m}$  at the same downstream distance  $500\mu\text{m}$ ). Diffusion of the liquid core resulted in not only broadening of MFD but also the attenuation of the optical power. Figure 3(b) shows that the liquid waveguide at  $Pe = 800$  experienced a  $0.14\text{ dB}$  attenuation while the liquid waveguide at  $Pe = 200$  experienced a  $1.06\text{ dB}$  attenuation at the same downstream distance  $500\mu\text{m}$ .

The change of MFD and the computed attenuation limit the distance over which the optical energy can be carried in the liquid element which is, of course, of primary concern in long distance communication applications. Although these effects may be reduced by using immiscible liquids, complete replacement of solid state optical components solely with liquid waveguides is likely not practical as current commercial optical fibers having attenuation values on the order of  $10\text{dB/km}$ . Thus the integration of the liquid and solid elements is crucial to realize a fluidically reconfigurable photonic chip.

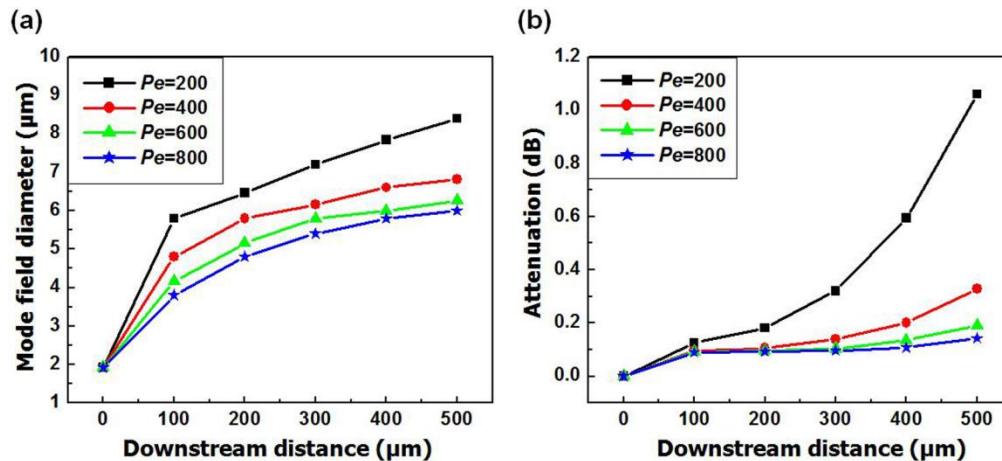


Fig. 3. (a) Mode field diameter at different Peclet numbers along the liquid waveguide. (b) Attenuation of optical power at different Peclet numbers along the liquid waveguide

### 3.2. Bending loss

In traditional solid core waveguides bends tighter than the critical radius can result in significant loss of optical power [19,20]. Although it has yet to be characterized, we expect similar behavior in liquid core waveguides. An additional dependence on Peclet number is also expected, analogous to the above. We note that for the simulations conducted here, the Dean number for the ranges from  $1.4 \times 10^{-2}$  to  $2.23 \times 10^{-1}$  and thus below the conditions where one would expect to observe Dean vortices in a fully 3D system. We therefore believe that our 2D model is valid for the conditions of interest here, however deviations from these trends are likely to be observed at much higher Pe numbers.

To characterize this we performed a series of simulations for the same liquid core system described above around a series of curved microchannels as shown in Fig. 4(a). To maintain consistency between each of the systems we made total length of the channels in each case the same distance,  $S_0 = 500 \mu\text{m}$ . Figure 4(b) shows the bending loss (dB) for different bending radii as a function of Peclet number. Similar to the bending loss in conventional solid waveguides, small bending radius decreased the power delivered through the bend. Higher Peclet numbers tended to reduce the bending loss due to its ability to confine the light more tightly (as described in section 3.1) and even in some cases a small radius bending with high Peclet number experienced less power loss than a large radius bending with low Peclet number.

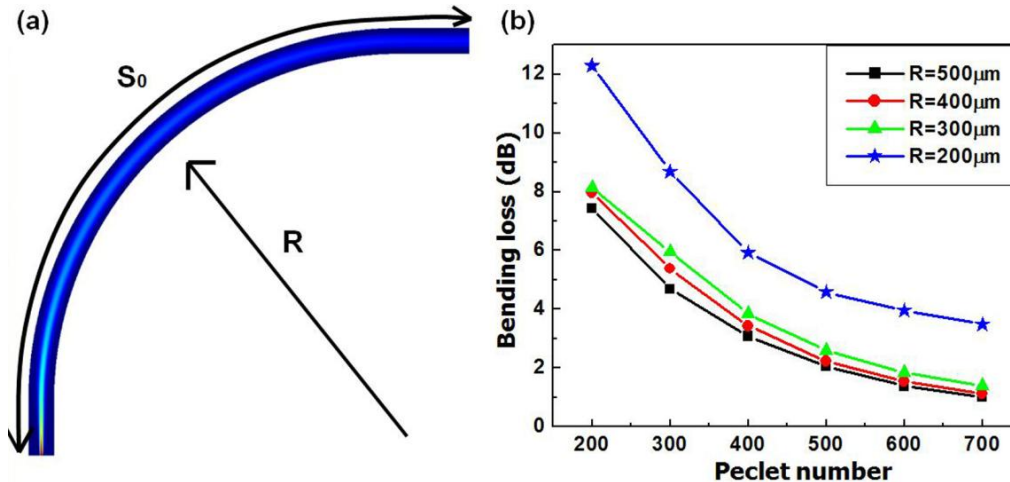


Fig. 4. (a) Refractive index profile in the curved channel with  $R = 500 \mu\text{m}$  and  $S_0 = 500 \mu\text{m}$  at  $Pe = 600$  (b) Bending loss at different Peclet numbers and different radii.

Diffusion of the liquid core in the curved liquid waveguide is faster than that in the straight liquid waveguide because of the deviation of flow velocity at the curve (“racetrack effect” [21]). Therefore two critical factors, bending radius and diffusion, make the optical power loss in the curved liquid waveguide more considerable than the straight one. At the same downstream distance,  $500 \mu\text{m}$ , and Peclet number,  $Pe = 600$ , the straight liquid waveguide had an attenuation value of  $0.19 \text{ dB}$  while the  $500 \mu\text{m}$  radius bend had  $1.38 \text{ dB}$ . Thus high Peclet number is recommended to minimize the bending loss in the liquid waveguide system with curves.

### 4. Results and discussion: liquid-to-solid light coupling

As mentioned above, optical coupling from the liquid state waveguide to the solid state waveguide represents the critical element of any future microfluidically reconfigurable photonic system. In this paper we investigate two forms of liquid to solid optical coupling

analogous to evanescent coupling and end-fire coupling in traditional solid state waveguides. In section 4.1 we study evanescent coupling in terms of coupling length and efficiency with various refractive indices of the solid waveguides and Peclet numbers of the liquid waveguides. In section 4.2 the efficiency of liquid to solid end-fire coupling is investigated. It is demonstrated that by optimizing the Peclet number of the liquid core waveguide, its mode field can be matched to that of the solid waveguide resulting in relatively efficient coupling.

#### 4.1. Evanescent coupling

Similar to evanescent coupling between solid waveguides, matching the propagation constants of the two waveguides is important for the evanescent coupling from the liquid core to solid core waveguides. The propagation constant is dependent on the geometrical dimensions and refractive index of a waveguide and thus, while remaining constant along the length of a solid core waveguide, changes as a function of downstream distance for a liquid core waveguide.

Figure 5(a) represents the concentration profile of the liquid waveguide as it flows alongside the test solid core waveguide. The solid waveguide has the same width as the liquid waveguide at the inlet and was located  $15\ \mu\text{m}$  offset from the inlet of the microchannel in the X-direction and  $1\ \mu\text{m}$  offset in the Y-direction. An additional flow was used from the top, a red arrow in Fig. 5(a), to close the gap between the liquid and solid waveguide resulting from boundary layers on the solid surface. As with the simulations above in all cases we used a  $500\ \mu\text{m}$  long simulation domain. Figure 5(b) shows the steady state electric field profile for the case of good coupling between the liquid and solid core waveguides.

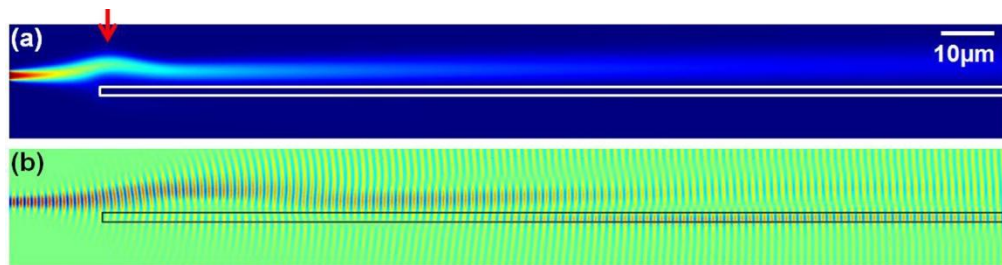


Fig. 5. (a, b) Concentration and steady state electric field profile at  $Pe = 500$ . RI of liquid waveguide at the inlet was 1.44 and solid waveguide was 1.37. Solid waveguide is represented as the white and black lines in Fig. 5(a) and 5(b)

Before continuing to our detailed analysis, we note here an interesting property of liquid to solid phase coupling. For evanescent coupling between solid waveguides, the light coupled into the second waveguide can be coupled back into the first waveguide as an overlapped radiation mode of the first waveguide perturbs the second waveguide [22]. In contrast, the coupling from the liquid to the solid waveguide is essentially irreversible since the liquid core diffuses downstream and the propagation constants are matched only over a certain distance. We can observe the irreversible coupling in Fig. 5(b) in which the coupled optical energy was locked in the solid waveguide.

We performed further numerical analysis by first, investigating the evanescent coupling by varying refractive index of the solid waveguide and second, by studying the effect of Peclet number of the liquid waveguide on the evanescent coupling. Figure 6(a) represents the cases that the RI of the liquid waveguide was fixed at 1.44 at the inlet and Peclet number was fixed at 250 while that of the solid waveguide was varied from 1.37 ( $\Delta n = -0.07$ ) to 1.43 ( $\Delta n = -0.01$ ). As mentioned above, varying the refractive index of the solid waveguide changes the required propagation constant of the liquid waveguide for light to be coupled into the solid waveguide. The light in the liquid waveguide was the fundamental mode and the coupled light in the solid waveguide was also the fundamental mode in the range investigated here.

As shown in the Fig. 6(a) the coupling length (*i.e.* the length measured from the start of the solid waveguide to the distance required for the light to be maximally coupled in the solid waveguide) became shorter as the RI of the solid waveguide become closer to that of the liquid waveguide. We observed that the coupling length was reduced to 10  $\mu\text{m}$  when the RI solid waveguide varied from  $\Delta n = -0.07$  to  $\Delta n = -0.01$ . Results shown in Fig. 6(b), which shows decrease in refractive index along the liquid waveguide, confirm our findings in Fig. 6(a).

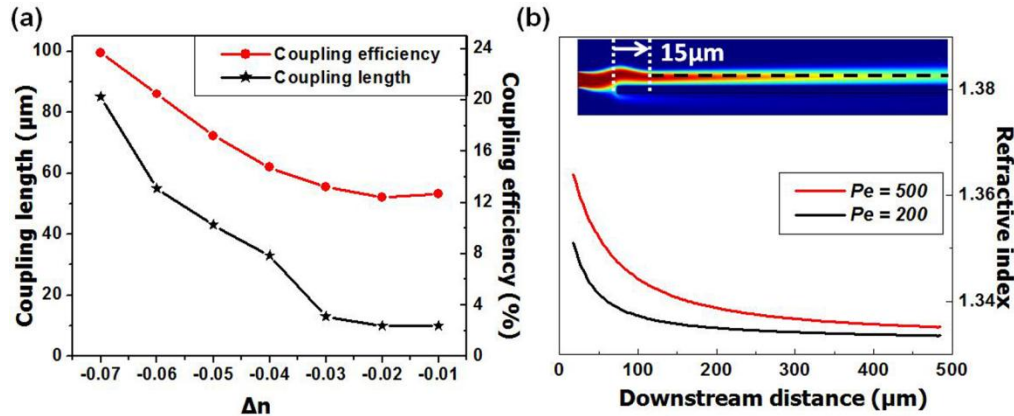


Fig. 6. (a) Coupling length (black) and coupling efficiency (red) as a function of  $\Delta n$  (RI of solid waveguide - RI of liquid waveguide) at  $Pe = 250$ . (b) Refractive index profile along liquid waveguide at  $Pe = 200$  (black) and 500 (red). The profiles were obtained along the black dotted line in the liquid waveguide and the X axis represents the downstream distance from the start of the solid waveguide.

The red line in Fig. 6(a) shows the coupling efficiency (defined as the ratio of the output power in the solid core waveguide to the input power of the liquid waveguide) as a function of  $\Delta n$  for the same Peclet number condition as those discussed above. In this fundamental mode coupling, the coupling efficiency decreased as the coupling length decreased. The shortening of the coupling length indicates that the propagation constant is matched further upstream where the refractive index changes more rapidly as seen in Fig. 6(b). As this matching occurs over only a short distance lower coupling efficiencies were obtained.

Figure 7(a) shows the coupling lengths and Fig. 7(b) the coupling efficiency as a function of Peclet number. The refractive index of solid waveguide ( $n_s$ ) varied between  $n_s = 1.37$  and  $n_s = 1.40$ . As shown in Fig. 7(a), the coupling length became longer as Peclet number becomes larger. For example, the coupling length increased from 75  $\mu\text{m}$  to 100  $\mu\text{m}$  when Peclet number of the liquid waveguide was changed from 200 to 500 at  $n_s = 1.37$ . Figure 7(b) shows an apparent different tendency from the previous results observed in Fig. 6(a) and 6(b) which showed reduced efficiencies as the coupling length decreased. This reversed trend is due to the faster change of propagation constants in the liquid core at higher Peclet number. The higher Peclet number resulted in the steeper gradient of the refractive index profile as seen in Fig. 6(b) and as a result a weakly matched propagation constant was coupled in the solid waveguide.

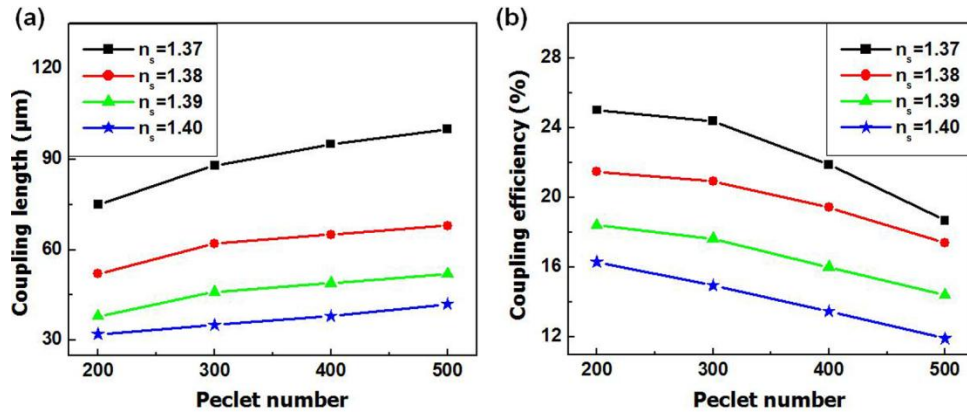


Fig. 7. (a, b) Coupling length and coupling efficiency at different Peclet numbers (200~500) with constant refractive indices (1.37~1.40) of the solid waveguide

To summarize, the evanescent coupling from the liquid to the solid waveguide was effectively irreversible due to the rapid downstream change in the propagation constant in the liquid waveguide. Compared to conventional solid state couplers which have the precisely computed overlap length and fixed geometries and refractive index profiles, to obtain the pre-designed division of optical power, the performance of our two-state evanescent coupler is not restricted by its original design and thus the amount of power coupling can be tuned.

#### 4.2. End-fire coupling

In section 3.1, we showed that the mode field diameter of the liquid waveguide varies according to the Peclet number of the system. Low Peclet number yielded broader concentration profiles and subsequently more weakly confined electric fields with larger mode field diameters.

Here, we exploit this tuning capability to achieve well matched MFD with that of the solid waveguide to demonstrate efficient end-fire coupling. In this case the liquid and solid waveguide were positioned along the same axis and began with the same 1.5  $\mu\text{m}$  width such that the liquid waveguide enveloped the solid waveguide as shown in Fig. 8(a) and 8(c). The inlet refractive index of the liquid waveguide was 1.44 and that of the solid waveguide was the same. Figure 8(a) and 8(b) show the concentration and the steady state electric field profiles at  $Pe = 200$  and Fig. 8(c) and 8(d) are at  $Pe = 800$ . The well matched MFD case was observed at  $Pe = 800$  showing how good coupling can be obtained.

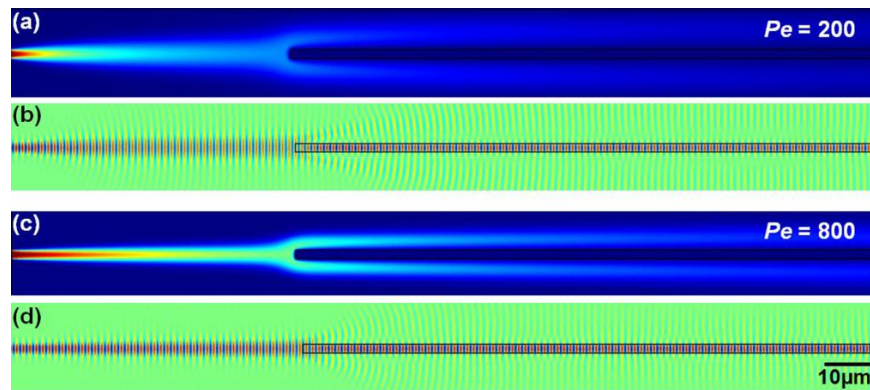


Fig. 8. (a, b) Concentration and steady state electric field profiles at  $Pe = 200$ . (c, d) Concentration and steady state electric field profiles at  $Pe = 800$ , RI of liquid waveguide at the inlet = 1.44 and RI of solid waveguide is the same.

Figure 9(a) shows the results of the end-fire coupling efficiency into the solid waveguide as a function of liquid waveguide Peclet number. As can be seen, lower Peclet number tended to yield lower coupling efficiencies than higher ones as the mode was more disperse when it reached the edge of the waveguide for coupling. The highest coupling efficiency recorded here is 84% at  $Pe = 1000$  (which was also the highest Peclet number tested) indicating that as Peclet number of the liquid waveguide becomes higher the MFD more closely matched that of the solid waveguide. This result does not imply necessarily that higher Peclet number achieves higher coupling efficiency. Figure 9(b) shows the coupling efficiency as a function of relative refractive index  $\Delta n$  (RI of the solid waveguide - RI of the liquid waveguide) at different Peclet numbers. We can observe that low Peclet number has higher coupling efficiency when the RI of solid waveguide is lower than that of the liquid waveguide as can be seen in the Fig. 9(b). In Fig. 9(b)  $Pe = 200$  had 57% coupling efficiency while  $Pe = 600$  had 38% when the RI of the solid waveguide is 0.08 less than that of the liquid waveguide.

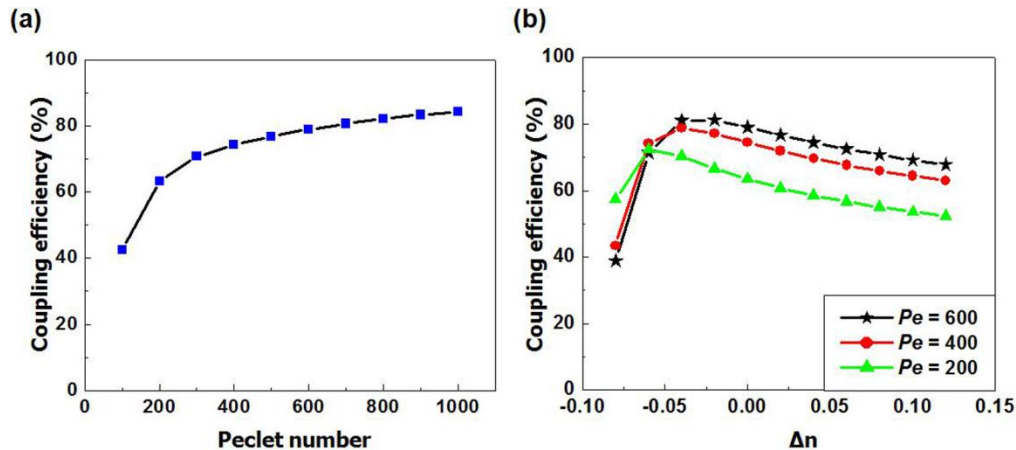


Fig. 9. (a) Coupling efficiency at different Peclet numbers with constant RI (1.44) of solid waveguide and liquid waveguide. (b) Coupling efficiency at different RIs of solid waveguide.

This adaptability to various refractive indices of solid waveguides makes the liquid waveguide a unique mode converter. In contrast to commercial optical fibers, the liquid waveguide can adjust the MFD of optical sources to be matched to that of a solid waveguide on a chip. Although higher coupling efficiency can be accomplished through prisms [23], gratings [24] and sophisticatedly designed converters [25], the liquid coupler has incomparable flexibility in the context of a universal converter.

## 5. Conclusions

In this paper, we have numerically investigated and characterized light propagation in liquid-core/liquid-cladding waveguides and light coupling from the liquid to the solid waveguides for cases of interest to the development of an optofluidically reconfigurable photonic system. We demonstrated that (1) instead of having a constant MFD and propagation constant as with conventional solid waveguides, the liquid waveguide's properties changed dramatically as a function of Peclet number and downstream distance due to diffusion of the liquid core, (2) that bending losses in liquid waveguide systems, even with very tight radii, could be reduced by increasing the waveguide Peclet number, (3) that evanescent coupling from the liquid to the solid waveguide was irreversible, and (4) that fluid end-fire coupling could have relatively high coupling efficiency when the tunable MFD of the liquid waveguide was matched to that of the solid waveguide. The numerical results obtained here provide valuable design data for the creation of several fluid-solid-optic components (*e.g.* optical switches, couplers, and splitters).

## **Acknowledgements**

This work was partially supported by the Air Force Office of Scientific Research through an STTR grant to Illuminaria LLC. under the Reconfigurable Materials for Cellular Electronic and Photonic Systems discovery challenge thrust and by the US National Science Foundation through grant NSF-CBET-0846489 “CAREER: Optofluidics - Fusing Microfluidics and Photonics.”